

Journal of Materials Chemistry C

Accepted Manuscript



This is an *Accepted Manuscript*, which has been through the Royal Society of Chemistry peer review process and has been accepted for publication.

Accepted Manuscripts are published online shortly after acceptance, before technical editing, formatting and proof reading. Using this free service, authors can make their results available to the community, in citable form, before we publish the edited article. We will replace this *Accepted Manuscript* with the edited and formatted *Advance Article* as soon as it is available.

You can find more information about *Accepted Manuscripts* in the [Information for Authors](#).

Please note that technical editing may introduce minor changes to the text and/or graphics, which may alter content. The journal's standard [Terms & Conditions](#) and the [Ethical guidelines](#) still apply. In no event shall the Royal Society of Chemistry be held responsible for any errors or omissions in this *Accepted Manuscript* or any consequences arising from the use of any information it contains.

Cite this: DOI: 10.1039/c0xx00000x

www.rsc.org/xxxxxx

ARTICLE TYPE

Synergistically-Controlled Nano-Templated Growth of Tunable Gold Bud-to-Blossom Nanostructures: A Pragmatic Growth Mechanism

Munmun Bardhan^a, Biswarup Satpati^b, Tanmay Ghosh^b, and Dulal Senapati,^{*a}

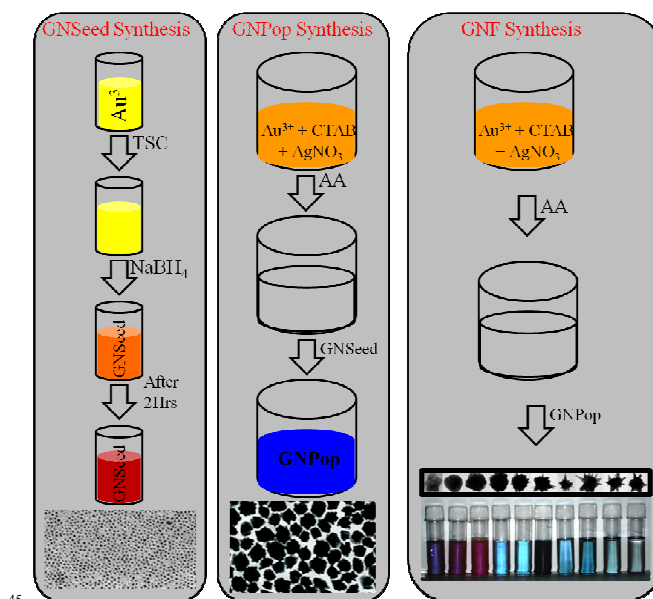
Received (in XXX, XXX) Xth XXXXXXXXXX 20XX, Accepted Xth XXXXXXXXXX 20XX

DOI: 10.1039/b000000x

A novel nano-templating method with a unique nanocrystal growth mechanism has been introduced for single pot production of size variable (110-360 nm), intrinsically-monodispersed, single-shaped, tunable plasmonic (580-1300 nm) gold nanomaterials showing the man made replica of nature's bud-to-blossom steps associated with gigantic SERS activity. In the first growth step we have synthesized 45 ± 3 nm gold nano-popcorns (GNPops) from 4.3 ± 1.4 nm spherical gold nano-seed and in the second growth step we used GNPops as templates for controlled overgrowth and to produce bigger gold nano-flowers (GNFs) simply by controlling the viscosity of the surfactant. TEM-based electron tomography (ET) of highly structured GNFs provides their actual morphology with no Bragg diffraction artefacts. Due to their broad plasmon tunability throughout the Vis-NIR region and extraordinarily high Raman activity these materials are suitable to find applications in tunable Plasmon spectroscopy, high-throughput Raman sensing and efficient photothermal therapy in the biological window.

INTRODUCTION

During the last few decades, there is a constant search for the methodologies to generate noble-metal nanomaterials with tailored size and shape¹⁻¹⁶ for harvesting embryonic physical^{17, 18}, chemical^{19, 20} and optoelectronic properties²¹⁻²³ to find their high throughput applications in different advanced fields⁵⁻¹² which includes sensing, diagnostics, therapeutic, optoelectronic, catalysis, alternate energy, etc. Though the literature is quite rich for standard methodologies to generate size variable metallic nanoparticles, good synthetic protocols for shape tailoring are not only rare^{13, 16, 24-26} but also very complicated for successful implementation. Most of these synthesis procedures start from the spherical seeds to develop much bigger structures with certain shape. Using this strategy different research groups throughout the globe including our group have synthesized different gold and silver nanomaterials in a single-pot-synthetic protocol^{13, 16, 27, 28}. It is vastly accepted and well documented in the literature that if the seed is small enough, it is easier to control the growth kinetics and vary the shapes of the nanomaterials from totally symmetric to highly directional nanoparticles. Compare to this, keeping the asymmetry same and growing much bigger structure with much more prominent sharp edges and tips suitable for electromagnetic field enhancement is rare in the literature. Moreover most of the developed seeded growth techniques are two-step seeding methods^{13, 16, 29} where the first step is the synthesis of spherical seed (diameter ~ 1-5 nm) and the second step is the growth of shape dependent anisotropic nanomaterials by using this seed. Besides that there are several reports where i) macromolecules



Scheme 1 Schematic presentation of Gold Nanoflowers (GNFs) synthesis. Three different steps of synthesis have been separated by three vertical column showing (i) synthesis of gold nanoseed ii) synthesis of GNPop and iii) synthesis of GNFs.

have been used as template to replicate the template's morphology³⁰, ii) polymer beads decorated with small silver seed particles were used as templates to grow gold nanoshells packed

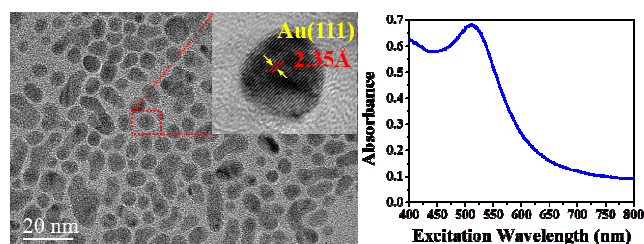


Figure 1 HRTEM and absorption spectrum of 4.3 ± 1.4 nm sized spherical gold nanoseed, used for icosahedral GNPoP synthesis in the first growth step.

with sharp spike shaped particles²⁶, iii) polystyrene bead supported Cu-nanoparticle as templates to fabricate highly branched gold nanoflowers (GNFs)²⁷, etc.

In this report, for the first time we have shown that a hierarchical nanoparticle itself can be used as an efficient template to guide the nanoparticle shape. Simply by varying the concentration of the surfactant we have controlled the kinetics of gold atoms deposition onto the template to overgrow much bigger replica of the starting material. As the kinetics becomes increasingly slow, we have achieved a replication of bud-to-blossom nanostructures. We have explained the growth mechanism of nano-flowering by considering synergistic effect of crystal facets free energy and CTAB-originated viscosity controlled Au^{3+} migration from CTAB molecules and subsequent reduction and deposition on GNPoP template surface as neutral gold atom (Au^0) for the development of preferential crystallographic planes. By using this multi step seeding-based nano-templating method we can generate nanomaterials with absolute plasmon tunability in the range 580-1300 nm in a single pot synthesis method. Moreover, synthetic procedure produces intrinsically-monodispersed single-shaped nanomaterials and we don't need any fractional separation to achieve highly pure nanoparticles. Besides that they show very high surface enhanced Raman scattering (SERS) activity and as we can make these hierarchical nanoparticles by using minimum amount of CTAB (minimum cytotoxicity), they are suitable for biological applications too.

EXPERIMENTAL SECTION

Chemicals

Chemicals including Gold (III) chloride trihydrate ($\text{HAuCl}_4 \cdot 3\text{H}_2\text{O}$) $\geq 99.9\%$ trace metal basis, Silver nitrate (AgNO_3) BioXtra $\geq 99\%$ (titration), Sodium borohydride (H_4BNa) granular, 10-40 mesh 98%, L-Ascorbic acid ($\text{C}_6\text{H}_8\text{O}_6$) ACS reagent $\geq 99\%$, and Hexadecyltrimethylammonium bromide or CTAB ($\text{C}_{19}\text{H}_{42}\text{BrN}$) assay $\geq 99\%$ (AT) were purchased from Sigma-Aldrich and used for the synthesis without any further purification. All the synthesis and experimental works have been done by using Milli-Q water.

Synthesis of gold nanoseed

Gold nanoflowers (GNFs) were synthesized by using multi step seeding-based nano-templating method where the final step seed was a nano template for predetermined tailored shape. In the first step we synthesized spherical gold nanoseed by adding 0.5 mL of

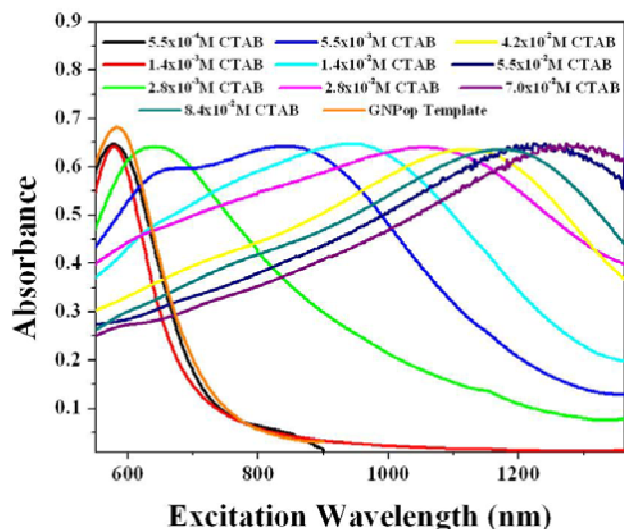


Figure 2 Tunable absorption spectra originating from bud-to blossom GNFs obtained by changing CTAB concentration in the range 5.5×10^{-4} M - 8.4×10^{-2} M. GNPoP has been used as nanotemplate in the synthesis.

10^{-2} M HAuCl_4 solution with 20 mL water in a small vial. Next 0.2 mL of 2.5×10^{-2} M Trisodium citrate solution was added drop wise and left for 1 min to mix well. Followed by 60 μL of 10^{-1} M ice cold freshly prepared NaBH_4 solution was added drop by drop which changes the solution colour from light yellow to light red. We kept this seed solution for another 2 hrs before using for the next synthesis step when the colour of the solution turns to deep red. Nanoseeds exhibit absorption spectra as shown in **Figure 1** with absorption maxima at 510 nm, which corresponds to 4.3 ± 1.4 nm seed, has been confirmed by TEM.

First growth step to synthesize GNPoPs

In the first growth step we have synthesized mono dispersed GNPoPs with average size 45 ± 3 nm. To synthesize GNPoPs, we dissolved 0.049 gm of CTAB in 45 mL water (2.8×10^{-3} M) by mild heating with constant slow stirring. To this solution 2 mL of 10^{-2} M HAuCl_4 solution was added and stirred for additional 1 min. Followed by 300 μL of 10^{-2} M freshly prepared AgNO_3 solution was added gently, mix well and then 320 μL 10^{-1} M ascorbic acid was added drop wise. As the solution became colourless, immediately 500 μL of gold nanoseed solution (as prepared) was added at a time. The solution became deep blue within a minute and left still for 2 hrs before using it for the next synthesis step. Details about the GNPoP synthesis has been mentioned elsewhere¹³.

Nano-templating step to synthesize GNFs

In the second growth step we have synthesized intrinsically monodispersed GNFs with size (diameter) variation between 110-360 nm. To synthesize different sized GNFs with differential petal openings we used 11 different growth solutions by dissolving 0.005, 0.01, 0.025, 0.05, 0.1, 0.25, 0.5, 0.75, 1.0, 1.25 and 1.5 gm of CTAB in 45 mL water by mild heating with constant stirring. To this solution 2 mL of 10^{-2} M HAuCl_4 solution was added and stirred for additional 1 min. Then 300 μL of 10^{-2} M freshly prepared AgNO_3 solution was added gently,

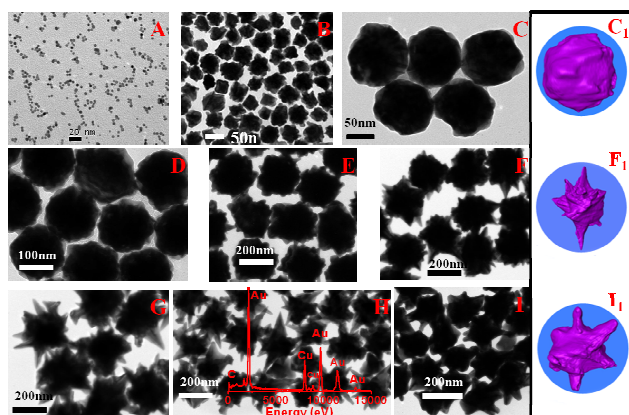


Figure 3 TEM images of: (A) Spherical Gold nano seed (4.3 ± 1.4 nm), (B) Gold NanoPopcorn, (C-I) GNFs at the CTAB concentration of 5.5×10^{-4} M, 2.8×10^{-3} M, 5.5×10^{-3} M, 1.4×10^{-2} M, 4.2×10^{-2} M, 5.6×10^{-2} M and 8.4×10^{-2} M. Inset EDX spectra shows that the GNFs are pure gold nanomaterials. C₁, F₁ and I₁ are the respective 3D-TEM-EM of C, F, and I.

mix well and then 320 μ L of 10^{-1} M ascorbic acid was added drop wise. As the solution became colorless, immediately 500 μ L of GNPpop solution was added at a time as nano-template and left the solution undisturbed for overnight to complete the growth process. Schematic representation of the nano-templated growth protocol for GNF synthesis is shown in **Scheme 1** where different growth solutions show different bright color.

UV-NIR absorption characterization

UV-Vis absorption spectra of the synthesized smaller GNFs have been recorded by using a Jasco V-650 spectrometer where as the Vis-NIR absorption spectra of the bigger GNFs have been recorded by using a PerkinElmer LAMDA 950 UV/Vis/NIR spectrophotometer. After synthesizing the GNFs, we have measured their UV-VIS-NIR absorption spectroscopy prior careful removal of unbound CTAB from the solution by using variable centrifugation speed between 1000-3000 rpm. We have performed three times controlled centrifugation for complete removal of CTAB from the solution without disturbing the surface-CTAB which is necessary for particle stabilization. Purified GNFs then used for absorption measurement. Normalized absorption spectra obtained from differently blossomed GNFs are depicted in **Figure 2**. Absorption spectra clearly imply that the described protocol is suitable for the application in tunable plasmon spectroscopy as we can tune the plasmon band in a broader range between 580-1300 nm.

TEM and SEM characterization

For High Resolution Transmission Electron Microscopic (HRTEM) measurements we used a FEI, Tecnai G2 F30, S-Twin microscope operating at 300 KV. High-angle annular dark field scanning/transmission electron microscopy (STEM-HAADF) is employed here using the same microscope, which is also equipped with a scanning unit and a HAADF detector from Fischione (model 3000). The compositional analysis was performed by energy dispersive X-ray spectroscopy (EDS, EDAX Instruments) attachment on the Tecnai G2 F30. For SEM measurement we used a Zeiss Supra 40, Field Emission SEM

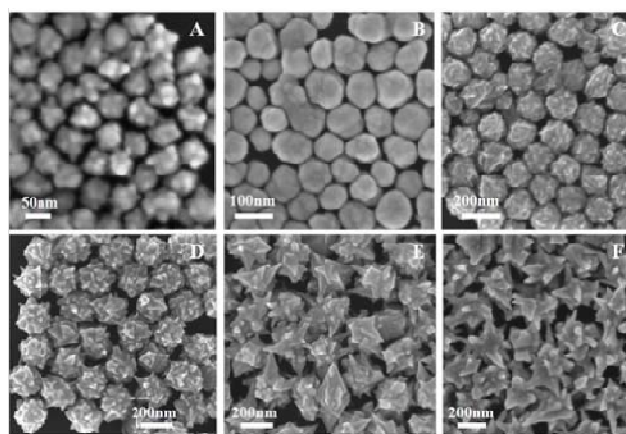


Figure 4 SEM images of: (A) GNPpop, (B) GNF at 5.5×10^{-4} M CTAB, (C) GNF at 1.4×10^{-3} M CTAB, (D) GNF at 2.75×10^{-3} M CTAB, (E) GNF at 2.8×10^{-2} M CTAB and (F) GNF at 5.6×10^{-2} M CTAB.

instrument. We have used simple but modified techniques for clean monolayer sample preparation both for TEM and SEM. For TEM measurement we used 300 mesh copper Formvar/carbon grid. We used dip-and-dry technique to make TEM samples. In this sample preparation technique we dip a TEM grid in the concentrated nanomaterial sample solution by using a tweezer and the hydrophobic carbon coating allow a monolayer of sample to stick on the copper mesh which we dry on a soft tissue paper. After complete drying we use this grid for TEM measurement. For SEM measurement we used polished silicon wafer as sample support. We inject about 20 μ L of the concentrated nanomaterial sample on the tilted silicon wafer and the hydrophobic nature of the wafer allows only a single layer of sample to stick on the surface which dries quickly to allow us for immediate SEM measurement. From the transmission electron microscopy (TEM) and scanning electron microscopy (SEM) measurements as shown in **Figure 3 & 4** respectively, it is evident that as we increase the concentration of CTAB in the final growth step, particles with bigger diameters are originating and resulting a gradual red shifting of the plasmon band. At very low concentration of CTAB (5.5×10^{-4} M to 2.8×10^{-3} M) we observe a single plasmon band and the corresponding TEM and SEM shows a near spherical shape of the overgrown template which we defined as the bud structure in the proposed bud-to-blossom steps. Compared to this, intermediate concentrations of CTAB (5.5×10^{-3} M to 1.4×10^{-2} M) show a double plasmon band indicating the development of the sharp tips or petals from the spherical core. Short wavelength plasmon band (near 650-700 nm) corresponds to the spherical core where as the long wavelength plasmon band (>800 nm) corresponds to the newly grown sharp petals. Since the petals are just started to grow from the core, we could expect reasonable contribution from both the core and petals towards the plasmon band and we can easily see two distinct plasmon bands. We define this step as half blossom GNFs. Further increments of CTAB concentration (2.8×10^{-2} M to 8.4×10^{-2} M) convert the absorption spectra again to a broad single banded plasmon. Corresponding TEM and SEM images of the GNFs shows predominant petal structure and due to their large structural features (average petal length: 60-100 nm) main

Cite this: DOI: 10.1039/c0xx00000x

www.rsc.org/xxxxxx

ARTICLE TYPE

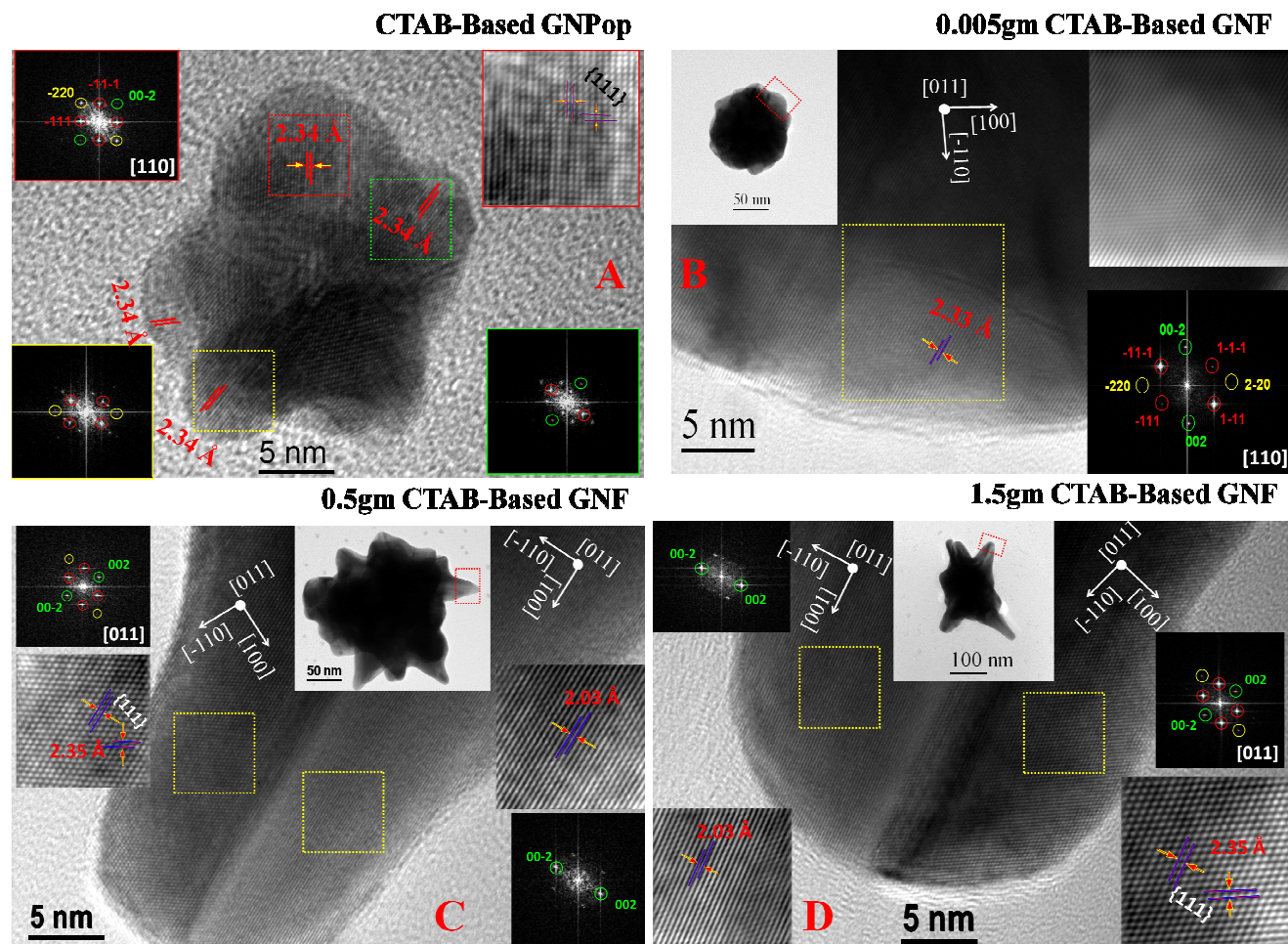


Figure 5 HRTEM of (A) Icosahedral GNPop as nano template, (B) 5.5×10^{-4} M CTAB-based GNF (unblossomed GNF), (C) 2.8×10^{-2} M CTAB-based GNF (fully blossomed GNF), and (D) 8.4×10^{-2} M CTAB-based GNF (blunted GNF).

5 contribution of the plasmon band comes from the petals and show a single plasmon band. Due to large distribution of petal size (0-200 nm) on each individual GNF, we observed broad absorption spectra.

RESULTS AND DISCUSSION

10 Our experimental results suggest that CTAB turned out to be the key controlling factor for bud-to-blossom steps of GNFs. In our previous report¹³ we used spherical gold nanoseed as the nucleation site and varied the CTAB concentration to generate different shaped gold nanoparticles in a single pot synthesis
15 procedure. Since the size of the seed was very small (4.3 ± 1.4 nm) and spherical in nature, it simply acts as the nucleation centre rather to acts as a template. In the present study we used 45 ± 3 nm size GNPs as the nucleation centre and their larger size

with defined morphology allow us to use the GNPs as the
20 effective template to over grow them to bigger GNFs simply by controlling the surfactant based viscosity. CTAB is water-soluble and has bromide counter ion which can be chemisorbed on these metal surfaces. CTAB has a sufficiently large head group to help the direction of crystal growth and a sufficiently long tail to make
25 a stable bilayer on the metal surface. The addition of AgNO_3 to CTAB in aqueous solution leads to immediate formation of AgBr (counter ion Br^- from CTAB molecules), which can play an important role in the shape control mechanism. It has been suggested that under potential deposition of metallic silver occurs
30 on the crystal facets of gold seed, leading to symmetry-breaking and multi-shape branched gold nanoparticle formation^{13, 30-34}. When the concentration of CTAB was varied from 5.5×10^{-4} M to 8.4×10^{-2} M and the other parameters are kept constant, their

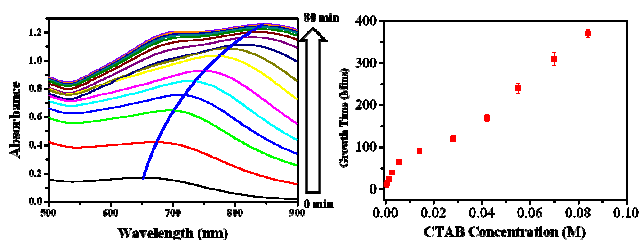


Figure 6 (Left) Time dependent absorption spectra of 5.5×10^{-3} M CTAB-based GNF, demonstrating growth kinetics and how the absorption profile changes with time during the formation of flower shaped nanoparticles, (Right) demonstrating how the growth time varies with the concentration of CTAB.

apparent shape (spiky nanosphere) remain constant but the size of the spikes or petals gradually increases with the CTAB concentration up to 6.7×10^{-2} M. Further increment of CTAB concentration results blunting of the petal tips which is clearly visible from TEM, SEM and 4π -angular ET view (**Figure 3I₁**). Corresponding absorption spectra of generated GNF at 8.4×10^{-2} M concentration of CTAB shows a blue shifting of the plasmon band from 1300 nm to 1180 nm indicates the blunting of petal tips.

Mechanism of Nano-Templated Growth of Tunable Gold Bud-to-Blossom Nanostructures

The growth of petals to replicate the bud-to-blossom steps is likely due to the interplay between the crystal facets free energy and CTAB-originated viscosity controlled Au^{3+} ion migration from CTAB molecules to GNP template surface and subsequent adsorption as Au^0 ($E_{\text{Au}^{3+}/\text{Au}^0}^0 = 1.5\text{V}$) after complete reduction. If we check the reduction potentials of Au^{3+} ions in different oxidation states ($E_{\text{Au}^{3+}/\text{Au}^+}^0 = 1.36\text{V}$, $E_{\text{Au}^{3+}/\text{Au}^0}^0 = 1.5\text{V}$, and $E_{\text{Au}^+/\text{Au}^0}^0 = 1.83\text{V}$), it is clear that though $\text{Au}^{3+} \rightarrow \text{Au}^+$ is a favourable path compared to $\text{Au}^{3+} \rightarrow \text{Au}^0$, unfavourable reduction potential for $\text{Au}^+ \rightarrow \text{Au}^0$ force Au^{3+} ions directly reduce to Au^0 (neutral gold atom) which is necessary for the generation of gold nano structures. During the past decade, with the continuous development of synthetic methodology of metal nanocrystals (NCs), researchers have learned that the morphology of metal NCs could be controlled by varying thermodynamic and kinetic parameters in solution-phase synthesis³⁵. Most noble metal NCs crystallize in the face-centered cubic (fcc) crystal structures and surface-energy considerations are crucial in understanding and predicting the morphology of noble-metal NCs. A close look into the formation mechanism of GNFs was achieved by characterizing using a high resolution transmission electron microscopy (FEI Tecnai F30 operating at 300 KV). Four different structures (GNPops as template and overgrowth GNFs at the CTAB concentration of 5.5×10^{-4} M, 2.8×10^{-3} M and 8.4×10^{-2} M) along with the 4.3 ± 1.4 nm spherical gold nanoseed were analyzed to understand the growth mechanism are presented in **Figure 5 & Figure 1** respectively. The corresponding HRTEM and fast Fourier transform (FFT) image in the inset for 4.3 ± 1.4 nm spherical gold nanoseeds (**Figure 1**) clearly indicates the crystalline nature of the structure is $\{111\}$. In **Figure 5A**, an icosahedral GNP template synthesized from 4.3 ± 1.4 nm spherical gold

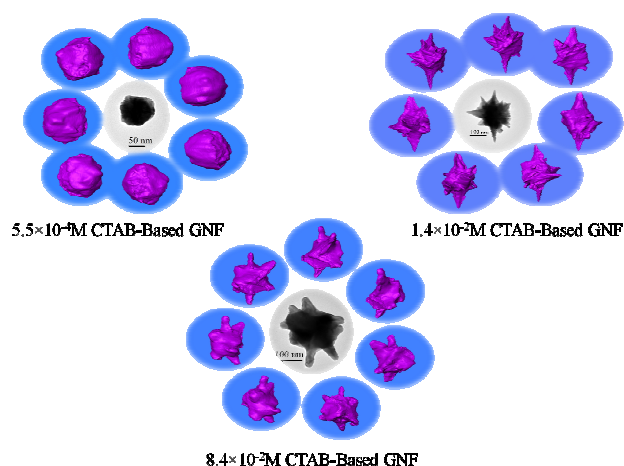


Figure 7 Electron tomography of 5.5×10^{-4} M, 1.4×10^{-2} M, and 8.4×10^{-2} M CTAB based GNFs. Black & White image corresponds to the 2D-TEM image and all the surrounding colored 3D images are reconstructed ET images in different orientation.

nanoseeds having all the tips oriented in $\{111\}$ direction, energetically most stable condition is having lowest free energies. According to literature, the free energies associated with the crystallographic planes of an fcc metal increases in the order: $\gamma(111) < \gamma(100) < \gamma(110)$ ³⁶. So, our result is consistent with the existing literatures to form the free energetically most stable structures both for spherical seed and for GNPops. In the case of 5.5×10^{-4} M CTAB-based product (bud shaped GNFs) the identified growth direction changed from $\{111\}$ to $\{110\}$ (**Figure 5B**) having the highest free energy and should have the tendency to change the crystal growth direction towards a lower surface energy configurations. In practice, however, kinetic considerations are also critical in determining nanocrystal morphology. This is particularly evident in colloidal synthesis, where parameters such as reaction time, capping agents, and reactant concentration profoundly affect nucleation and growth. It is a known observation that the presence of CTAB can retard the rate of reduction of gold by a factor of 100-1000 depending on the concentration of CTAB^{13, 37}. This retardation of Au^{3+} reduction is due to the binding of the gold ions to the cationic CTAB micells³⁸. So, CTAB not only directs gold to deposit on selected crystal facets but also drastically retards the rate of metallic gold (Au^0) formation. CTAB molecules have a stronger affinity for unstable $\{110\}$ facets than other facets^{16, 31-32}. Because of this preferential adsorption of CTAB associated with the lower viscosity of the medium (5.5×10^{-4} M CTAB), system favours unhindered migration of Au atoms to isotropically grow all the petals of GNPops to form bud-structure with predominant crystal facets of $\{110\}$. As we increase the concentration of CTAB, unstable crystal growth direction changes from highest free energetic crystallographic direction $\{110\}$ to the energetically most favourable direction $\{111\}$ along with the restricted migration of Au^{3+} and subsequent reduction to Au^0 at higher viscosity to push them preferentially adsorb on relatively stable $\{100\}$ facets. The lattice fringe pattern observed in the HRTEM image (**Figure 5C**), the corresponding fast Fourier transform (FFT) image and the inverse FFT in the inset clearly

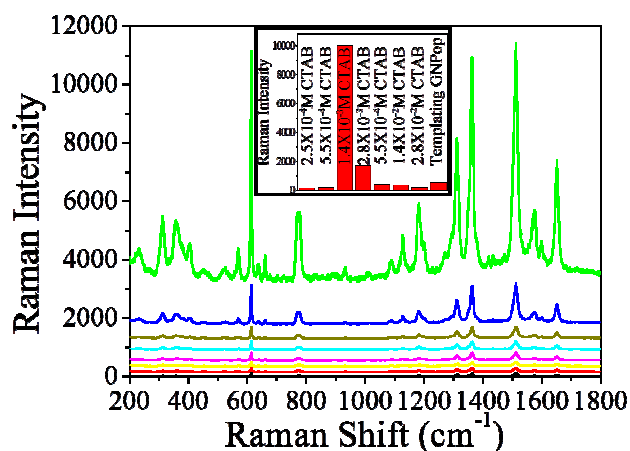


Figure 8 SERS spectra from different steps of bud-to-blossom GNPs compared with the SERS intensity from templating GNPp in presence of Rh6G as Raman tag. Inset is a bar plots of SERS activity from different GNPs as we vary the CTAB concentration.

indicate the crystalline nature of the structure. Remarkably, we have observed the change in growth direction from $\{110\}$ to a mixture of $\{100\}$ and $\{111\}$ facets (one half of the tip in the growth direction shows $\{100\}$ facet while other half shows $\{111\}$ facet) in case of 2.8×10^{-2} M CTAB added product (half blossomed GNF) as we expected from the free energy point of view. This observation is same for all analyzed tips of the half blossom GNF, even from different half blossomed GNPs, which clearly indicates that the system has moved to its lower surface energy configurations. Due to higher atom addition rate on high energy facets, high-energy facets can easily disappear during crystal growth and only low-energy facets can survive as because high-energy facets having highly unsaturated coordination of surface atoms³⁵. The growth direction remains same (i.e. a mixture of $\{100\}$ and $\{111\}$) for the case of 6.7×10^{-2} M and 8.4×10^{-2} M CTAB-based fully blossomed GNPs (**Figure 5D**). From free energy point of view though we were expecting to achieve the full blossomed GNPs with $\{111\}$ facets, competing higher viscosity of CTAB preferentially push the Au^{3+} to migrate and subsequently reduce to Au^0 towards relatively stable $\{100\}$ facets and as a result of this combined effects the fully blossomed GNPs to settle with an optimum structure having a mixture of $\{100\}$ and $\{111\}$ facets. So, our results show that it is a synergistic effect of crystal facets free energy and CTAB-originated viscosity controlled Au^{3+} migration for the development of preferential crystallographic planes. This simplified nano-templated growth technique will find enormous applications in the near future to synthesize overgrown nanostructures for any predetermined shape. Additionally, the presence of twin planes in the individual tips illustrates the fact that, these structures are not simply complex manifoldness of single crystalline tips contrary to present literature³⁹. Moreover, we also confirm from the TEM and SEM (**Figure 3 & 4**) images that the number of petals and their lengths strongly depends on the average diameter of the GNPs, with more number of petals and much bigger petals grown on the larger particles. It has also been noticed that as the diameter of the GNPs increases, the core size is gradually reduces. This might be due to the

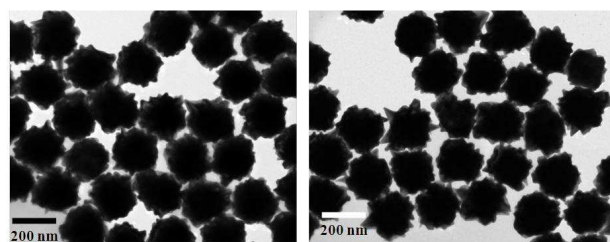


Figure 9 TEM images of 2.8×10^{-3} M CTAB-based GNPs (left) in absence of Rh6G and (right) in presence of Rh6G.

50

accommodation of more number of petals on expense of the core surface. To understand the role of CTAB concentration in growth process, we have studied the growth time for differently blossomed GNPs. It's been clearly visible from our study (**Figure 6**) that the growth time gradually increases as we increase the concentration of CTAB for making GNPs in the growth step. This phenomenon has been explained before as the controlling factor for the production of Au^0 by Au^{3+} reduction due to the binding of the gold ions to the cationic CTAB micells³⁴. So, CTAB not only directs gold to deposit on selected crystal facets but also drastically retards the rate of metallic gold (Au^0) formation. Each GNF's structural statistics is given in **Table 1** with finer details. Interestingly, we have also observed from the HRTEM images that branching out of petals occurs as a consequence of gradual twinning, so that in all cases the GNPs ultimately comprise a polycrystalline core with a number of single twined crystal petals branching out from the surface. It should be pointed out that these complex nanostructures are extremely stable at room temperature.

70

3D Transmission electron microscopy-based electron tomography (3D TEM-ET) of gold nano flowers

75

In general, a precise three-dimensional (3D) nanometrological characterization is prerequisite for correlation to optical properties and calculation of band structure can now be performed at the single nanoparticle level using TEM. In common practice, the morphological features of NPs are inferred from TEM because it provides the required high-spatial resolution and have become a conventional technique. Although there is a set of powerful techniques routinely available in a transmission electron microscope, the vast majority provide only 2D "projection" of the morphology in the form of images or thickness maps. TEM-ET is a technique of growing importance for 3D crystallographic and metrological studies of different kinds of nanostructures facilitates avoiding Bragg diffraction artifacts inherent in 2D images. To overcome this problem and to find out their actual morphology in a true sense, we have performed tomography of our newly synthesized GNPs. Electron tomography of different steps of bud-to-blossom GNPs have been performed where the 3D electron tomographic view of 5.5×10^{-4} M (nanobud), 1.4×10^{-2} M (fully blossomed), and 8.4×10^{-2} M (over blossomed) CTAB-based GNPs have been shown in **Figure 7**. It is well documented in **Figure 7** that at very low concentration of CTAB (5.5×10^{-4} M) petals are developing from the core and these sharp features looks more like petals than pointed tips. When we increase the concentration of CTAB to 1.4×10^{-2} M, petals are well developed with sharp features but

95

Cite this: DOI: 10.1039/c0xx00000x

www.rsc.org/xxxxxx

ARTICLE TYPE

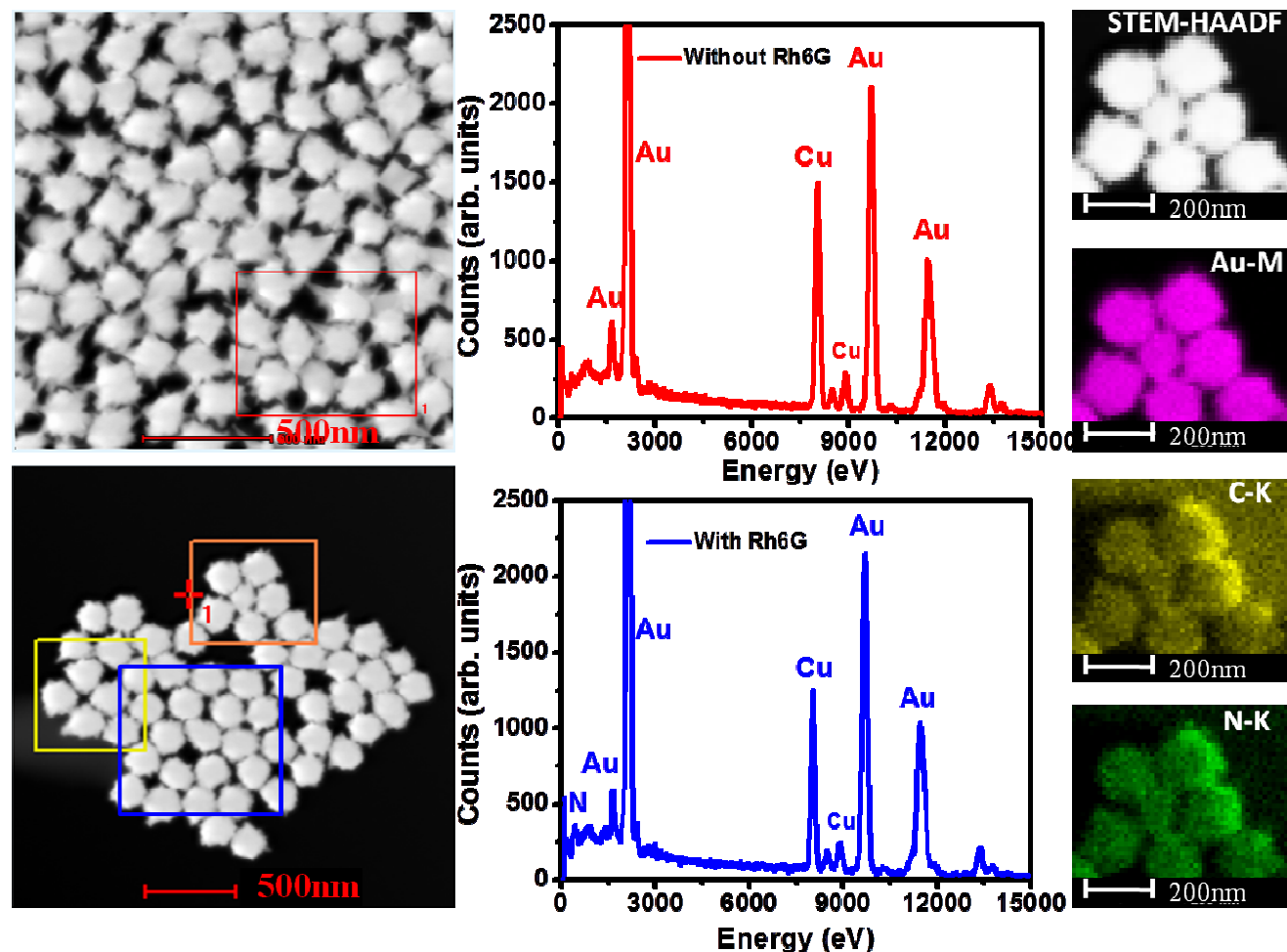


Figure 10 Elemental mapping of the 2.8×10^{-3} M CTAB-based GNPs. Top left: TEM image of GNF without Rh6G and Top middle: EDX of GNF without Rh6G. Bottom left: TEM image of GNF with Rh6G and Bottom middle: EDX of GNF with Rh6G. Rightmost column shows the elemental mapping of GNF in presence of Rh6G.

further increment of CTAB concentration to 8.4×10^{-2} M for over blossomed GNF shows blunting of the sharp petals as we have already discussed previously in the experimental section. So, the 3D TEM-ET results clearly show that we can increase the CTAB concentration up to a certain limit (7.0×10^{-2} M for 45 ± 3 nm GNPop nano-template) to grow the petals of GNPs but beyond that concentration the adsorption of more CTAB and Au⁰ on the petals forced them to transform into rounded shape to avoid from crumbling. Since the tomographic measurement is a time consuming study, we have considered 3-4 particles for each differently blossomed GNPs to measure the structural parameters as listed in **Table 1**.

Surface enhanced Raman scattering activity of GNPs

To find out the bio-chemical applications of our synthesized

GNPs we have checked their surface enhanced Raman scattering (SERS) activity by using a Horiba Jobin-Yvon LabRAM Raman microscope with excitation wavelength at 632.8 nm. Along with the absorption and fluorescence-based techniques, SERS is another nanoparticle-based spectroscopic technique has been studied extensively in the last few decades⁴⁰⁻⁴⁴ and promised to be one of the most useful techniques for the future applications in diagnosis and sensing⁴⁵⁻⁴⁶. The usefulness of this technique lies in its ability to provide the chemical signature along with its signal amplification (10^8 – 10^{14} order) leads to state-of-the-art highly specific and sensitive assay for diagnosis, detection and monitoring⁴⁵⁻⁴⁶. Though bulk SERS enhancements have been understood as largely plasmon-based^{17, 50} since the first experimental demonstrations⁴⁷, resonance^{48, 51} and chemical contributions^{49, 52} can also be quite large under certain conditions.

Cite this: DOI: 10.1039/c0xx00000x

www.rsc.org/xxxxxx

ARTICLE TYPE

Table 1 GNFs structural statistics which explains how the particle diameter, core diameter, number of petals on each GNF and average length of petals changes with CTAB concentration

| CTAB Concentration (M) | Core Diameter (nm) | Average Diameter (nm) | Average No. of Petals | Individual Average Petal Length (nm) | Absorbance (nm) | Growth time (min) |
|------------------------|--------------------|-----------------------|-----------------------|--------------------------------------|-----------------|-------------------|
| 2.8×10^{-4} | 110±6 | 110±3 | 0 | 0 | 577 | 10 |
| 5.5×10^{-4} | 120±5 | 120±6 | 0 | 0 | 577 | 15 |
| 2.8×10^{-3} | 140±6 | 175±7 | 15 | 15 | 640 | 40 |
| 5.5×10^{-3} | 172±4 | 290±4 | 30 | 60 | 660 & 840 | 65 |
| 1.4×10^{-2} | 160±5 | 300±5 | 40 | 70 | 950 | 92 |
| 2.8×10^{-2} | 155±3 | 330±6 | 54 | 85 | 1059 | 120 |
| 4.2×10^{-2} | 145±5 | 345±3 | 60 | 90 | 1126 | 170 |
| 5.5×10^{-2} | 140±7 | 360±4 | 68 | 105 | 1230 | 240 |
| 8.4×10^{-2} | 135±4 | 275±6 | 45 | 70 | 1180 | 370 |
| GNPop | 25±5 | 45±3 | 60 | 10 | 584 | 10 |

In the present set of experiment we have used Rhodamine 6G (Rh6G) as the analyte to measure the offered Raman cross section from our synthesized GNFs and has been shown in **Figure 8**. It is evident from **Figure 8** that the Raman scattering cross section of Rh6G on GNFs is substantially higher than that on the templating GNPops. The bar plot in **Figure 8** inset shows how SERS intensity changes with CTAB concentration and gives a relative estimation of enhancement compared to GNPpop used for nano-templating. The Raman enhancement, G , is measured experimentally by direct comparison as shown in Equation (1)^{40, 44, 53-54}.

$$G = (I_{\text{SERS}}/I_{\text{Raman}}) \times ([M_{\text{Bulk}}]/[M_{\text{Ads}}]) \quad (1)$$

In which I_{SERS} is the intensity of a 1511 cm^{-1} vibrational mode in the SERS spectrum of Rh6G in presence of GNF, and I_{Raman} is the intensity of the same mode in the bulk Raman spectrum from Rh6G alone. M_{Bulk} is the number of molecules used in the bulk, M_{Ads} is the number of molecules adsorbed and sampled on the SERS-active substrate. All spectra are normalized for integration time. The enhancement factor estimated from the SERS signal is approximately 1.9×10^{10} which is one order more compared to the templating GNPpop⁴⁰. Several factors are responsible for this gigantic Raman cross-section which include: (a) much bigger surface area of GNFs compared to GNPpop to hold more number of analytes on their surface, (b) enormous number of petals on the nanosurface with pointed tips and sharp edges offers the focusing of the electromagnetic field at their apexes, which will provide a sufficient electromagnetic field enhancement, (c) close-by petals, inter-petal space or the space between the core and petals acts as active pockets which we define as nano-pockets to trap dye molecules and form natural hotspot without making any aggregates and finally, (d) low concentration of surfactant will allow Rh6G to surface adsorb efficiently for maximum Raman enhancement. Extent of surfactant (or CTAB thickness on GNFs) is a crucial controlling factor for observed Raman cross section of Rh6G on different GNFs. From **Figure 8** and the inset we can

clearly observe that the Raman signal intensity increases gradually as we increase the CTAB concentration in the concentration range: $2.5 \times 10^{-4} \text{ M}$ to $1.4 \times 10^{-3} \text{ M}$. In this low concentration of CTAB, gradual increment of CTAB concentration makes the overgrown structures bigger and bigger with more structured petals and causes steady increment of Raman signal. Once the petals are fully formed, more amount of CTAB will make a thick layer of surfactant on the GNFs and will not allow Rh6G to come close to the surface for efficient SERS effect. We have performed controlled absorption and TEM study to find out the role of petals on SERS enhancement. In our experiment we have mixed 10^{-8} M GNF solutions with 10^{-5} M Rh6G and varied the GNF: Rh6G volume ratios. From the measured absorption spectra of GNFs in presence of Rh6G does not show any noticeable aggregation and indirectly proves that most of the Rh6G molecules trapped in the inter-petal nano-pockets to form hot spot and enhances the Raman signal significantly. Higher concentration of CTAB doesn't allow free Rh6G molecules to adsorb on the petal tips to cause any considerable aggregation. To confirm the existence of inter-petal nano-pockets in our GNFs we have recorded the TEM images of GNFs before and after the addition of Rh6G as shown in **Figure 9**. It is clear from the TEM images that added Rh6G doesn't cause any aggregation. Moreover, elemental mapping of the GNFs (**Figure 10**) shows a substantial enhancement of nitrogen content (EDX plot) specifically on the GNF surface after the addition of Rh6G. The presence of nitrogen as an element on GNFs can come from both CTAB and Rh6G and enhancement of nitrogen content after the addition of Rh6G proves strong presence of Rh6G on GNF surface. Since Rh6G molecules adsorb on the GNFs surface and enhance Raman cross section of Rh6G significantly without making any noticeable aggregation, the only possible way to hold Rh6G molecules are in the inter-petal nano-pockets.

CONCLUSION

In conclusion, we have reported a nano-popcorn (GNPop) templated gold nanoflower (GNF) synthesis and proposed a unique nanocrystal growth mechanism by considering synergistic effect of crystal facet free energy and CTAB-originated viscosity controlled Au³⁺ migration. We strongly believe that this simplified nano-templated technique will find universal applications to synthesize any predetermined overgrown nanostructure. Size variable GNFs show the man made replica of nature's bud-to-blossom steps with size tunability of the particles between 110-360 nm and the length tunability of the petals between 10-100 nm. Moreover, these particles are intrinsically mono-dispersive and are extremely stable (months) under ambient condition. We have also presented TEM-ET of highly structured GNFs to find out their actual morphological transition in a true sense while changes the morphology from bud shaped to fully blossomed GNF. Our synthesized GNFs show gigantic Raman enhancement suitable to use them effectively for high throughput Raman sensing and their tunable plasmon characteristics throughout the VIS-NIR region (580-1300 nm) allow us to apply them as efficient photothermal agent in the biological window.

ACKNOWLEDGEMENT

We thank BARD project under the Department of Atomic Energy (DAE, India Government) for generous funding for this research work. DS wishes to give special thanks to Prof. Tapas Chini and co-workers, SPMS Division, SINP for SEM measurements; Prof. P. M. G. Nambissan and Mrs. Soma Roy, NAP Division, SINP for NIR measurements; and Dr. Manash Ghosh, IACS, Kolkata for SERS measurements.

Notes and references

^a Nanophotonics Group, Room-105, Chemical Sciences Division, Saha Institute of Nuclear Physics, 1/AF, Bidhannagar, Kolkata-700064, India.. Fax: +91-33-2337-4637; Tel: +91-33-2337-0463 (Ext: 1105); Email: dulal.senapati@saha.ac.in

^b Surface Physics & Material Science Division, Saha Institute of Nuclear Physics, 1/AF, Bidhannagar, Kolkata-700064, India.. Fax: +91-33-2337-4637; Tel: +91-33-2337-0463 (Ext: 4215)

† Electronic Supplementary Information (ESI) available: See DOI: 10.1039/b000000x/

1. E. Roduner, *Chem. Soc. Rev.* 2006, **35**, 583.
2. H. Duan and S. Nie, *J. Am. Chem. Soc.* **129**, 2412-2413 (2007).
3. W. -L. Huang, C. -H. Chen and M. H. Huang, *J. Phys. Chem. C* 2007, **111**, 2533.
4. Y. Khalavka, J. Becker and C. Sönnichsen, *J. Am. Chem. Soc.* 2009, **131**, 1871.
5. Y. Yin, C. Erdonmez, S. Aloni and A. P. Alivisatos, *J. Am. Chem. Soc.* **128**, 12671-12673 (2006).
6. A. Courty, A. -I. Henry, N. Goubet and M. -P. Pileni, *Nat. Mater.* 2007, **6**, 900.
7. W. Niu, S. Zheng, W. Wang, X. Liu, H. Li, S. Han, J. Chen, Z. Tang and G. Xu, *J. Am. Chem. Soc.* 2009, **131**, 697.
8. M. Oh and C. A. Mirkin, *Nature* 2005, **438**, 651.
9. A. Ohnuma, E. C. Cho, P. H. C. Camargo, L. Au, B. Ohtani and Y. Xia, *J. Am. Chem. Soc.* 2009, **131**, 1352.
10. J. Wu, S. C. Mangham, V. R. Reddy, M. O. Manasreh and B. D. Weaver, *Sol. En. Mat Sol. Cell.* 2012, **102**, 44.
11. T. K. Sau, A. L. Rogach, F. Jäckel, T. A. Klar and J. Feldmann, *Adv. Mater.* 2010, **22**, 1805.
12. C. Hrelescu, T. K. Sau, A. L. Rogach, F. Jäckel and J. Feldmann, *Appl. Phys. Lett.* 2009, **94**, 153113.
13. D. Senapati, A. K. Singh and P. C. Ray, *Chem. Phys. Lett.* 2010, **487**, 88.
14. C. Ziegler and A. Eychmuller, *J. Phys. Chem. C* 2011, **115**, 4502.
15. S. J. Tan, M. J. Campolongo, D. Luo and W. Cheng, *Nat. Nanotech.* 2011, **6**, 268.
16. T. K. Sau and C. J. Murphy, *J. Am. Chem. Soc.* 2004, **126**, 8648.
17. M. Moskovits, *M. Rev. Mod. Phys.* 1985, **57**, 783.
18. L. Wang, Z. Zhang and X. Han, *NPG Asia Materials* 2013, **5**, e40.
19. The Chemistry of Nanomaterials: Synthesis, Properties and Applications, Editor(s): C. N. R. Rao, A. Muller and A. K. Cheetham, Wiley-VCH Verlag GmbH & Co. KGaA, 2005.
20. P. Mulvaney, in Nanoscale Materials in Chemistry, ed. K. Klabunde, Wiley-VCH, Weinheim, 2001, p. 121.
21. C. -W. Tseng and Y. -T. Tao, *J. Am. Chem. Soc.* 2009, **31**, 12441.
22. K. -S. Cho, E. K. Lee, W. -J. Joo, E. Jang, T. -H. Kim, S. J. Lee, S. -J. Kwon, J. Y. Han, B. -K. Kim, B. L. Choi and J. M. Kim, *Nature Photon.* 2009, **3**, 341.
23. Y. Wu, Y. Li, B. S. Ong and P. Liu, *Adv. Mater.* 2005, **17**, 184.
24. C. G. Khoury and T. Vo-Dinh, *J. Phys. Chem. C*, 2008, **112**, 18849.
25. B. L. Sanchez-Gaytan, Z. Qian, S. P. Hastings, M. L. Reza, Z. Fakhraai and S. -J. Park, *J. Phys. Chem. C* 2013, **117**, 8916.
26. M. Pradhan, J. Chowdhury, S. Sarkar, A. K. Sinha and T. Pal, *J. Phys. Chem. C* 2012, **116**, 24301.
27. C. J. Murphy, *Science* 2002, **298**, 2139.
28. Q. Zhang, N. Li, J. Goebel, Z. Lu and Y. Yin, *J. Am. Chem. Soc.* 2011, **133**, 18931.
29. T. K. Sau and C. J. Murphy, *Langmuir* 2004, **20**, 6414.
30. M. Salsamendi, P. A. G. Cormack and D. Graham, *New J. Chem.* 45 2013, **37**, 3591.
31. M. Liu and P. Guyot-Sionnest, *J. Phys. Chem. B* 2005, **109**, 22192.
32. M. Grzelczak, J. Pérez-Juste, P. Mulvaney and L. M. Liz-Marzán, *Chem. Soc. Rev.* 2008, **37**, 1783.
33. Z. Li, W. Li, P. H. C. Camargo and Y. Xia, *Angew. Chem. Int. Ed.* 2008, **47**, 9886.
34. H. Zhang and D. Wang, *Angew. Chem. Int. Ed.* 2008, **47**, 3984.
35. A. R. Tao, S. Habas and P. Yang, *Small* 2008, **4**, 310.
36. Z. L. Wang, *J. Phys. Chem. B.* 2000, **104**, 1153.
37. J. Perez-Juste, L. M. Liz-Marzan, S. Carnie, D. Y. C. Chan and P. Mulvaney, *Adv. Funct. Mater.* 2004, **14**, 571.
38. K. Esumi, K. Matsuhisa and K. Torigoe, *Langmuir* 1995, **11**, 3285.
39. P. Senthil Kumar, I. Pastoriza-Santos, B. Rodríguez-González, F. J. G. de Abajo and L. M. Liz-Marz'an, *Nanotechnology* 2008, **19**, 015606.
40. W. Lu, A. K. Singh, S. A. Khan, D. Senapati, H. Yu and P. C. Ray, *J. Am. Chem. Soc.* 2010, **132**, 18103.
41. C. L. Haynes, C. R. Yonzon, X. Zhang and R. P. Van Duyne, *J. Ram. Spec.* 2005, **36**, 471.
42. L. X. Quang, C. Lim, G. H. Seong, J. Choo, K. J. Do, S. -K. Yoo, *Lab Chip* 2008, **8**, 2214.
43. T. Vo-Dinh, F. Yan and M. B. Wabuyele, *J. Ram. Spec.* 2005, **36**,

| | |
|---|-----|
| 640. | 65 |
| 44. D. Senapati, S. S. R. Dasary, A. K. Singh, T. Senapati, H. Yu and P. C. Ray, <i>Chem. Eur. J.</i> 17 , 8445-8451 (2011). | |
| 45. R. A. Alvarez-Puebla and L. M. Liz-Marzan, <i>Small</i> 2010, 6 , 604. | |
| 46. P. J. Vikesland and K. R. Wigginton, <i>Environ. Sci. Technol.</i> 2010, 44 , 3656. | 70 |
| 47. M. Fleischmann, P. J. Hendra and A. J. McQuillan, <i>Chem. Phys. Lett.</i> 1974, 26 , 163. | |
| 48. A. B. Myers and R. A. Mathies, In <i>Biological applications of Raman spectroscopy</i> ; Spiro, T. G., Ed.; Wiley and Sons: New York, 1987; pp 1. | 75 |
| 49. A. Otto, In <i>Light Scattering in Solids IV</i> ; Cardona, M. G., G., Ed.; Springer-Verlag: Berlin, 1984; Vol. 4 , 289-418. | |
| 50. S. Zou and G. C. Schatz, <i>Chem. Phys. Lett.</i> 2005, 403 , 62. | 80 |
| 51. A. B. Myers, <i>Acc. Chem. Res.</i> 1997, 30 , 519. | |
| 52. B. N. J. Persson, <i>Chem. Phys. Lett.</i> 1981, 82 , 561. | 15 |
| 53. L. Brus, <i>Acc. Chem. Res.</i> 2008, 41 , 1742. | |
| 54. F. Casadio, M. Leona, J. R. Lombardi and R. Van Duyne, <i>Acc. Chem. Res.</i> 2010, 43 , 782. | 85 |
| | |
| 20 | 90 |
| | |
| 25 | 95 |
| | |
| 30 | 100 |
| | |
| 35 | 105 |
| | |
| 40 | 110 |
| | |
| 45 | 115 |
| | |
| 50 | 120 |
| | |
| 55 | 125 |
| | |
| 60 | 130 |
| | |
| | 135 |

Cite this: DOI: 10.1039/c0xx00000x

www.rsc.org/xxxxxx

ARTICLE TYPE

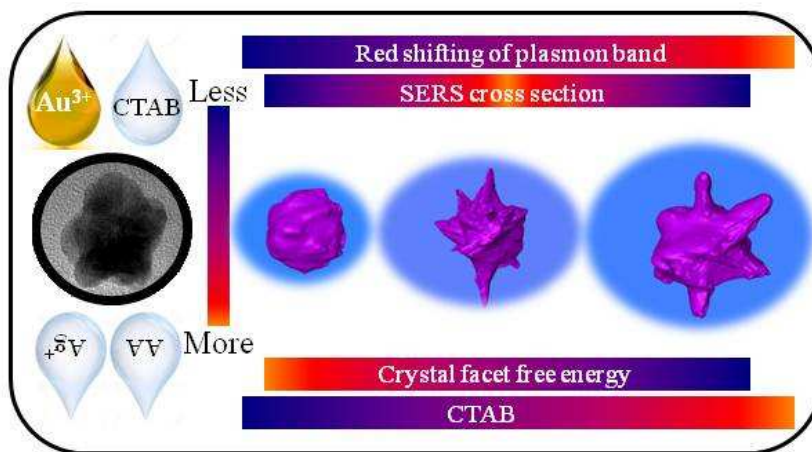


Table of Contents: Nano-templating method with pragmatic nanocrystal growth mechanism explains the production of size-variable, intrinsically monodispersed, tunable bud-to-blossom plasmonic (580-1300 nm) gold-nano-flowers.

5

10

15

20